Investigating the physicochemical characteristics of monovalent metal-doped nickel oxide thin films

C. Maghni[a,b,*] , C. Zaouche[c], L. Dahbi[d], S. Saggai[e], E. Guedda[e]
[a]*Faculty of Science and Technology, University Mohammed chérif messaadia BP 1553 Souk Ahras 41000, Algeria*
[b]*Physico-chemistry of Materials and Environment Laboratory, Ziane Achour University of Djelfa, BP 3117, Djelfa, Algeria*
[c]*Material Sciences Department, Faculty of Science, University of Biskra, 07000 Biskra, Algeria*
[d]*Teacher Education College of Setif, Messaoude Zeghar, Algeria*
[e]*Higher School of Saharan Agriculture – El Oued, PB 90 Chouhada, El Oued 39011, Algeria*

The effect of Ag doping on the optical, structural, and electrical properties of deposited $Ni_{1-x}Ag_xO$ thin films deposited on glass substrates by spray pyrolysis has been studied. This work aims to investigate the optical and physical characteristics variations of $Ni_{1-x}Ag_xO$ thin films fabricated into semiconductors with varying doping levels x. The values of 0 at.%, 2 at.%, 4 at.%, 6 at.%, and 8 at.% are these levels. The transmission spectra demonstrate the good optical transparency of the $Ni_{1-x}Ag_xO$ thin films in the visible range of 70% to 85%. The thin films of $Ni_{1-x}Ag_xO$ exhibited optical gap energies ranging from 3.63 to 3.71eV. Between 329 and 430meV was the range of the Urbach energy. Nonetheless, numerous flaws with the highest Urbach energy are observed in $Ni_{0.92}Ag_{0.08}O$ thin films. The lowest optical gap energy is found in $Ni_{0.92}Ag_{0.08}O$ thin sheets. A maximum of $0.024(\Omega.cm)^{-1}$ electrical conductivity was observed in the $Ni_{0.92}Ag_{0.08}O$ thin films. Our films have an average electrical conductivity of approximately $0.0176(\Omega.cm)^{-1}$. The $Ni_{1-x}Ag_xO$ thin film XRD patterns show that the films have a cubic structure and are polycrystalline.

(Received November 16, 2023; Accepted March 1, 2024)

Keywords: Nickel oxide, Monovalent metal, Doping, Optical gap energy, Urbach energy, Thin films

1. Introduction

Nickel oxide is one of the most important semiconductor materials in the environmental field because of its ability to detect toxic gases [1]. Nickel oxide (NiO) has several different applications in the fields of piezoelectric, optoelectronic, environmental, and renewable energy, such as sensors, fuel cell electrodes, catalysis, thermoelectric devices, dye-sensitized solar cells (DSSCs), and electro-chromic materials for displays [2–8]. Moreover, it is used to find suitable materials with enhanced properties for gas sensing applications for detecting the sensibility in the environment such as NO_x, SO_x, CO, and CO_2…, at high temperature. Because of its semiconductor nature and its ability to control optical transparency and electrical conductivity, determining the form of the applied interaction is important. However, several studies have found that NiO has high optical transparency and good electrical conductivity under various experimental conditions. NiO thin films have a direct band gap ranging from 3.5 to 4.3eV [9–10].

Several techniques, such as molecular beam epitaxial (MBE), electrochemical deposition, pulsed laser deposition (PLD), chemical vapor deposition, spray Sol–Gel processes, and spray pyrolysis, can be used to deposit nickel oxide in thin layers [11–17]. To enhance their optical and electrical characteristics, we used argent-doped NiO thin films.

*Corresponding author: c.maghni@univ-soukahras.dz
https://doi.org/10.15251/DJNB.2024.191.359

Because of the rare earth material quality caused by the rise in optical band gap energy (broadening) of this metal transition in the periodic table, it was employed in the research.

In this study, we used spray pyrolysis at 500°C to create Ag-doped NiO thin films on a glass substrate. This glass substrate was sprayed for 6min. Ag-doped NiO thin films for $Ni_{1-x}Ag_xO$ were synthesized at various doping concentrations (0, 2, 4, 6, and 8 at. %). The optical and electrical properties of the deposited thin films were improved by the introduction of $Ni_{1-x}Ag_xO$ thin films. Nonetheless, we examined how $Ni_{1-x}Ag_xO$ thin films produced as semiconductors alter their optical, structural, and electrical characteristics.

2. Experimental procedure

$Ni_{1-x}Ag_xO$ solutions were prepared by dissolving nickel acetate ($Ni(CH_3.CO_2)_2.4H_2O$) and argent acetate ($AgC_2H_3O_2$) in 0.5 mol l^{-1}. In this study, we used Ag doping with various concentrations in the game Ag/Ni = 0, 2, 4, 6, and 8 at.% or (x = 0, 0.02, 0.04, 0.06, and 0.08). Next, we added a drop of HCl to stabilize the heating solution. The mixture solution was stirred at room temperature and heated at 40 °C for 2 h to yield a clear and transparent solution. The coating was prepared 1 day after the precursor was prepared.

The $Ni_{1-x}Ag_xO$ samples were prepared by spraying the coating solution onto a glass substrate. Its temperature is 500°C for 6 min to obtain a thin film. The prepared $Ni_{1-x}Ag_xO$ thin films at different Ag doping levels were 0 at.%, 2 at.%, 4 at.%, 6, and 8 at.%. After the deposition of the thin layers, we left the substrate to decrease its temperature to that of the room.

The structural properties of $Ni_{1-x}Ag_xO$ thin films were studied using X-ray diffraction (XRD Bruker AXS-8D) with CuKa radiation (λ=0.15406nm) in the scanning range of (1h) which was between 20° and 70°. The optical transmission of the deposited films was measured in the range of (300–900nm) by using an ultraviolet– visible spectrophotometer (LAMBDA 25), and the electrical conductivity was measured by four-point methods.

3. Results and discussion

3.1. Structural properties of $Ni_{1-x}Ag_xO$ thin films

The structural characterization of the $Ni_{1-x}Ag_xO$ thin films is carried out by X-ray diffraction method that is shown in figure 1. The polycrystalline structure of the films, according to the XRD spectra, is of the cubic type of NiO (JCPDS) No. 73-1519) [18]. The XRD peaks in Figure 1 are located at 37.40° and 43.14° and correspond to the (111) and (200) crystal planes, respectively. The peak position is consistent with the findings of Rahman et al. [19]. In thin films, we found that at x=0.08, the intensity of the (111) and (002) peaks increased as the doping level x increased. The optimal orientation is along the (111) and (002) planes, as confirmed by this information. However, the film at x=0.08 has higher and sharper diffraction peaks, indicating an enhancement of crystallinity compared with other films.

The structure information was defined by the diffraction peak angles of the Ag-doped NiO thin films (seeTable 1). The lattice parameter **a** of Ag-doped NiO thin films was calculated from the XRD patterns using the following equation [20]:

$$\frac{1}{d_{hkl}^2} = \frac{h^2+k^2+l^2}{a^2} \quad (1)$$

where $\boldsymbol{h}$, $\boldsymbol{k}$ and $\boldsymbol{l}$are the Miller indices of the planes. $\boldsymbol{a}$is the lattice parameter and $\boldsymbol{d_{hkl}}$ is the interplanar spacing. The crystallite sizes $\boldsymbol{G}$ of (111) and (200) planes were calculated according to the Scherer equation [21- 22]:

$$G = \frac{0.9\lambda}{\beta \cos\theta} \quad (2)$$

where$\boldsymbol{G}$is the crystallite size, $\boldsymbol{\beta}$is the full width at half-maximum (FWHM), $\boldsymbol{\theta}$is Bragg angle of the diffraction peaks and $\boldsymbol{\lambda}$is the X-ray wavelength (λ=0.15406nm). The variations are shown in Tables 1 and 2.

The variations of the crystallite size and diffraction angle according to (111) and (200) peaks presented in Figure 2a and 2b show the variation of crystallite size and diffraction angle of Ag doped NiO thin films as a function of Ag doping level. Table 1 shows that when the doping level x increased from 0.04 to 0.08, the diffraction angles of the (111) plan decreased, as shown in Figure 2a. As one can observe from Table 1, the (111) plan's crystallite size shrank to its lowest value at x=0.04. In contrast, figure 2b demonstrates that as doping levels x increased, the diffraction angles of the (200) plan declined, climbed, and then decreased again, ultimately reaching their maximum value at x=0.08(see Table 2). However, we observed that the crystallite size of the (200) plan decreased to a minimum value at x=0.04. The improvement in the crystallinity and a-axis orientation of the Ag-doped NiO thin films suggested a decrease in the crystallite size. A number of these occurrences have been noted in [23–27]. This outcome can be explained by thin-layer crystallites coalescing to enhance oxygen transport [28].

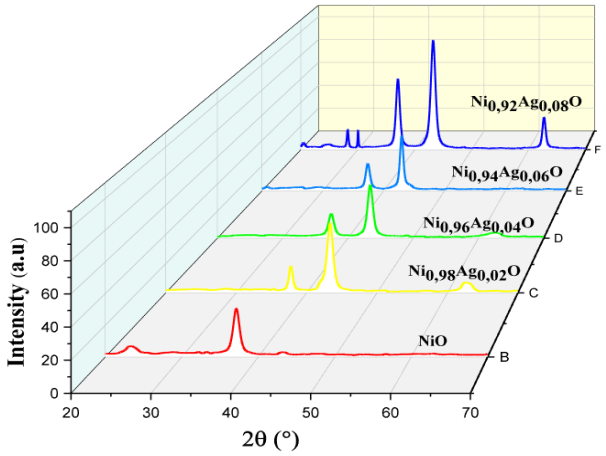

Fig. 1. X-ray diffraction of $Ni_{1-x}Ag_xO$ thin films as a function of Ag doping level

Table 1. The structural parameters of $Ni_{1-x}Ag_xO$ thin film as a function of Ag doping level of (111) diffraction peak.

X	2θ(°)	d (nm)	$\beta_{1/2}$ (°)	G(nm)	a(nm)
0	37.4492	0,24007	0.4047	20.7364	0,415816
0.02	37.4092	0,24031	0.6409	13.0926	0,416244
0.04	37.5294	0,23957	0.9557	8.7831	0,414959
0.06	37.4473	0,24008	0.7983	10.5123	0,415836
0.08	37.1748	0,24178	0.6409	13.0836	0,418776

Table 2. The structural parameters of $Ni_{1-x}Ag_xO$ thin film as a function of Ag doping level of (200) diffraction peak.

x	2θ(°)	d (nm)	$\beta_{1/2}$ (°)	G(nm)	a(nm)
0	42.9178	0,21066	0.3260	26.1954	0,421324
0.02	42.9164	0,21067	0.4834	17.6658	0,421337
0.04	43.4541	0,20818	0.7983	10.7172	0,416371
0.06	42.9550	0,21049	0.6409	13.3262	0,420976
0.08	43.4809	0,20806	0.2473	34.5989	0,416126

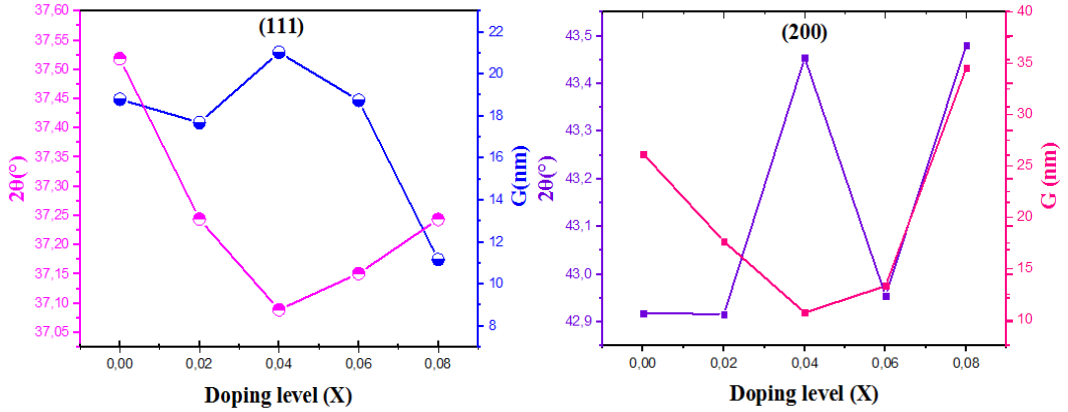

(a) *(b)*

Fig. 2. The variation of crystallite size and diffraction angle of Ag doped NiO thin films according to a (111) phase and b (200).

3.2. Optical properties of $Ni_{1-x}Ag_xO$ thin films

As shown in Figures 3 and 4, optical characterization of the synthesized $Ni_{1-x}Ag_xO$ thin films by doping levels x was performed by measuring the transmittance and absorbance in the wavelength region of 300–900nm. As we can see, the spray $Ni_{1-x}Ag_xO$ thin films have an average transmission of almost 75% in the visible spectrum. In contrast to other doping levels x, which are found between 355 and 370nm, the region of the absorption edge for these levels was situated between 320 and 370nm [29–30]. The space between the conduction and valence bands is the absorbance fluctuation for the $Ni_{1-x}Ag_xO$ thin films as shown in Figure 4. At wavelengths less than 370 nm, absorption edge shifts were detected. With an increase in the doping level x, $Ni_{1-x}Ag_xO$ thin film absorption edge shifts increased. The doping level x influences the optical characteristics of $Ni_{1-x}Ag_xO$ thin films.

The role of doping levels x in the transmission of thin films of $Ni_{1-x}Ag_xO$ was observed in the thin film quality due to the higher transparency. High transparency was obtained in the Ag-doped NiO thin film at 6% because of the interstitial sites of Ag and Ni. The absorbance and optical band gap energy E_g of fabricated $Ni_{1-x}Ag_xO$ thin films were determined by the following relations [31–33]:

$$A = \alpha d = -\ln T \tag{3}$$

$$(Ahv)^2 = C\left(hv - E_g\right) \tag{4}$$

where $\boldsymbol{A}$ is the absorbance of fabricated $Ni_{1-x}Ag_xO$ thin films, α is the absorption coefficient, d is the film thickness, T is the transmission of fabricated $Ni_{1-x}Ag_xO$ thin films, C is a constant, $h\upsilon$ is the energy of photon ($h\upsilon = \frac{1240}{\lambda(\mathrm{nm})}(\mathrm{eV})$) and E_g is the band gap energy of the semiconductor. However, the disorder or Urbach energy (E_u) was also determined by the following expression[34– 35]:

$$A = A_0 \exp\left(\frac{h\upsilon}{E_u}\right) \tag{5}$$

where$\boldsymbol{A_0}$ is a constant, $h\upsilon$ is the energy of the photon, and E_u is the Urach energy. The sequence of the flaws was characterized by the tail width of the Urbach energy. Figure 5 shows the changes in the optical band gap energy and Urbach energy of the synthesized $Ni_{1-x}Ag_xO$ thin films as a function of the doping level x. It was found that the band gap energy was less than 3.72eV. With an increase in the doping levels from 3.63 to 3.71eV, the band gap energy value varied. Because of the reduction in the size of the crystallites in the manufactured $Ni_{1-x}Ag_xO$ thin films, the effect of quantum confinement may be used to highlight the decrease in the optical band gap energy value (see Figure 2).As can be seen in Figure 5, the Urbach energy value increased and decreased with the increase in doping levels from 329 to 430meV. This can also be related to the diminution of the crystallite size value (see Figure 2).

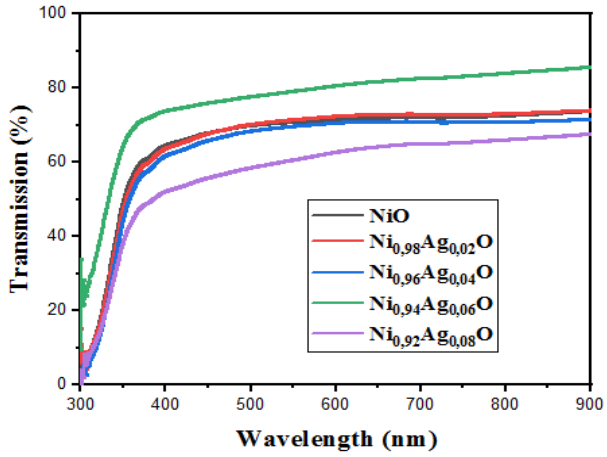

Fig. 3. Transmission spectra of $Ni_{1-x}Ag_xO$ thin films as a function of Ag doping level.

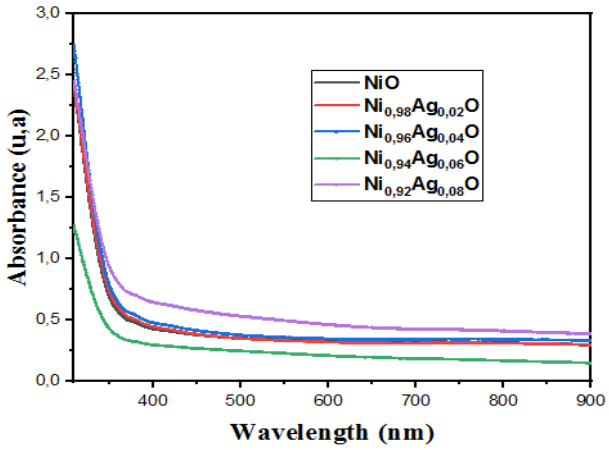

Fig. 4. Absorbance spectra of $Ni_{1-x}Ag_xO$ thin films as a function of Ag doping level.

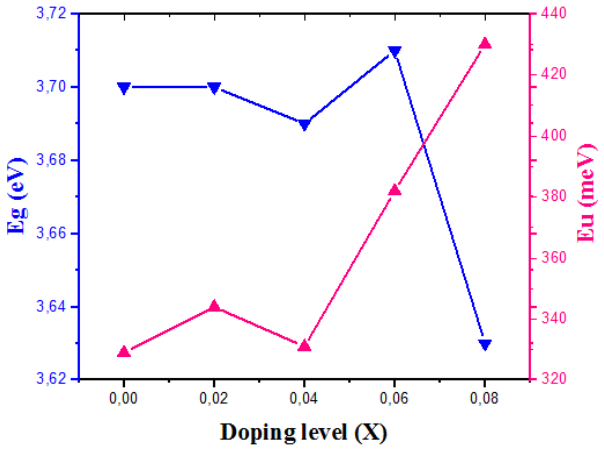

Fig. 5. The variations of optical pand gap energy and Urbach energy of Ag doped NiOthin films at various doping levels.

3.3. Electrical properties of $Ni_{1-x}Ag_xO$ thin films

The four-points probe method was used to determine the electrical conductivity of $Ni_{1-x}Ag_xO$ thin films. It is based on measuring the sheet resistance of the films as expressed by:

$$R_{sh} = \frac{\pi}{\ln(2)} \cdot \frac{V}{I} \tag{6}$$

Where I is the applied currant I=1nA and V is the measurement voltage. However, the electrical conductivity σ is also determined by the following equation:

$$\sigma = \frac{1}{d.R_{sh}} \tag{7}$$

Figure 6 shows the variation in the electrical conductivity of Ag-doped NiO thin films as a function of the Ag doping level. As can be seen, the electrical conductivity increases with increasing Ag doping level up to 8 at.%, where we obtained a maximum conductivity value of $0.024(\Omega.cm)^{-1}$. The increase in the conductivity of the $Ni_{1-x}Ag_xO$ thin films can be explained by the displacement of electrons. The latter comes from the Ag+ donor ions in the substitution sites of Ni+2 and the formation of molecular $NiAg_2O$ on the surface. The increase in the conductivity of the deposited films after 6 at.% can be related to the increase in the potential barriers because the introduced atoms are segregated into the grain boundaries [36-37]. Figures2, 5, and 6 show the decrease in the crystallite size, the decrease in the optical gap energy, the increase in the Urbach energy, and the increase in the electrical conductivity. These results explain the good crystallization of the thin films according to [38–41].

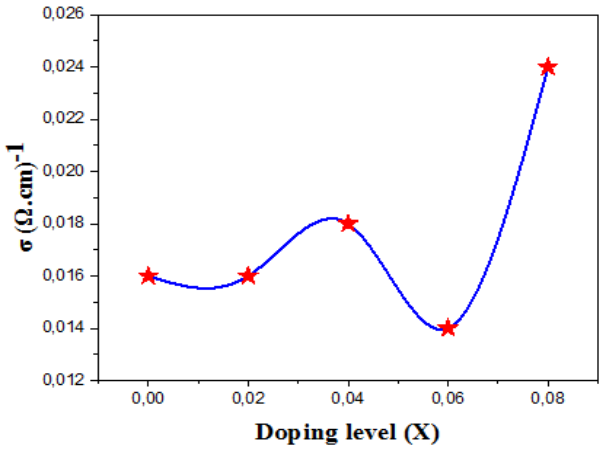

Fig.6. The electrical conductivity variation of $Ni_{1-x}Ag_xO$ thin films as a function of Ag doping level.

4. Conclusion

In this work, nickel acetate and argon acetate were used in spray pyrolysis to successfully deposit argon-doped nickel oxide thin films (Ag/Ni = 0, 2, 4, 6, and 8 at. %) on glass substrates. In the visible spectrum, the $Ni_{1-x}Ag_xO$ thin films exhibit transparency. The energy of the optical gap varies from 3.63 to 3.71eV. The Urbach energy fluctuates between 329 and 430meV. That being said, $Ni_{0.92}Ag_{0.08}O$ thin films show many flaws at the maximal Urbach energy. Thin films of $Ni_{0.92}Ag_{0.08}O$ have the lowest optical gap energy. The $Ni_{0.92}Ag_{0.08}O$ thin films also exhibited the highest electrical conductivity. The crystallite sizes of the $Ni_{0.96}Ag_{0.04}O$ films range from 8.7831nm (111) at the minimum to 10.7172nm (200) at the peak. The XRD patterns of the $Ni_{1-x}Ag_xO$ thin films indicate that the films are polycrystalline with a cubic structure. The electrical conductivity of the deposited films is on the order of $0.0176(\Omega.cm)^{-1}$. Figures 2, 5, and 6 show the decrease in the crystallite size, the decrease in the optical gap energy, the increase in the Urbach energy, and the increase in the electrical conductivity. These results explain the good crystallization of the thin films.

References

[1] V. Verma, M. Katiyar, Thin Solid Films 527, 369(2013); https://doi.org/10.1016/j.tsf.2012.12.020

[2] S. C. Chen, T. Y. Kuo, Y. C. Lin, H. C. Lin, Thin Solid Films 519(15), 4944(2011); https://doi.org/10.1016/j.tsf.2011.01.058

[3] R. Sharma, A. D. Acharya, S. B. Shrivastava, M. M. Patidar, M. Gangrade, T. Shripathi, V. Ganesan, Optik 127(11), 4661(2016); https://doi.org/10.1016/j.ijleo.2016.01.050

[4] S. Benramache, M. Aouassa, Journal of Chemistry and Materials Research 5(6), 119(2016).

[5] S. Dendouga, S. Benramache, S. Lakel, Journal of Chemistry and Materials Research 5(4), 78(2016).

[6] D. Dini, Y. Halpin, J. G. Vos, E. A. Gibson, Coordination Chemistry Reviews 304-305, 179(2015); https://doi.org/10.1016/j.ccr.2015.03.020

[7] G. F. Cai, C. D. Gu, J. Zhang, P. C. Liu, X. L. Wang, Y. H. You, J. P. Tu, ElectrochimicaActa 87, 341(2013); https://doi.org/10.1016/j.electacta.2012.09.047

[8] A. C. Nwanya, S. U. I. Offiah, C. Amaechi, S. Agbo, S. C. Ezugwu, B. T. Sone, R. U. Osuji, M. Maaza, F. I. Ezema, ElectrochimicaActa 171,128(2015); https://doi.org/10.1016/j.electacta.2015.05.005

[9] R. Romero, F. Martin, J. R. Ramos-Barrado, D. Leinen, Thin Solid Films 518(16), 4499(2010);

https://doi.org/10.1016/j.tsf.2009.12.016
[10] T. Chtouki, L. Soumahoro, B. Kulyk, H. Bougharraf, B. Kabouchi, H. Erguig, B. Sahraoui, Optik 128, 8(2017); https://doi.org/10.1016/j.ijleo.2016.10.007
[11] R. J. Deokate, R. S. Kalubarme, C. J. Park, C. D. Lokhande 224, 378(2017); https://doi.org/10.1016/j.electacta.2016.12.034
[12] Y. Yu, X. Li, Z. Shen, X. Zhang, P. Liu, Y. Gao, T. Jiang, J. Hua, Journal of Colloid and Interface Science 490, 380(2017); https://doi.org/10.1016/j.jcis.2016.11.037
[13] S. U. Offiah, M. O. Nwodo, A. C. Nwanya, S. C. Ezugwu, S. N. Agbo, P. U. Ugwuoke, R. U. Osuji, M. Malik, F. I. Ezema, Optik 125, 2905(2014); https://doi.org/10.1016/j.ijleo.2013.11.073
[14] S. C. Chen, T. Y. Kuo, Y. C. Lin, S. W. Hsu, H. C. Lin, Thin Solid Films 549, 50(2013); https://doi.org/10.1016/j.tsf.2013.07.017
[15] X. H. Xia, J. P. Tu, J. Zhang, X. L. Wang, W. K. Zhang, H. Huang, ElectrochimicaActa 53(18), 5721(2008); https://doi.org/10.1016/j.electacta.2008.03.047
[16] I. Castro-Hurtado, J. Herra'n, G. G. Mandayo, E. Castan˜o, Thin Solid Films 520(3), 947(2011); https://doi.org/10.1016/j.tsf.2011.04.180
[17] C. Zaouche, Y. Aoun, S. Benramache, A. Gahtar, Scientific Bulletin of valahia University materials and mechanics 17(17), 27(2019);https://doi.org/10.2478/bsmm-2019-0015
[18] J. Cao, Z. Wang, R. Wang, S. Liu, T. Fei, L. Wanga, T. Zhang, Materials Chemistry A 3(10), 5635(2015); https://doi.org/10.1039/C4TA06892K
[19] M. AbdurRahman, R. Radhakrishnan, R. Gopalakrishnan, Alloys and Compounds 742, 421(2018); https://doi.org/10.1016/j.jallcom.2018.01.298
[20] A.F. Saleh, Application or Innovation in Engineering & Management 2(1), 16 (2013).
[21] A. Gahtar, S. Benramache, A. Ammari, A. Boukhachem, A. Ziouche, Inorganic and Nano-Metal Chemistry 52(1), 112(2022); https://doi.org/10.1080/24701556.2020.1862225
[22] A. Gahtar, C. Zaouche, A. Ammari, L. Dahbi, Chalcogenide Letters 20(5), 377(2023); https://doi.org/10.15251/CL.2023.205.377
[23] N. Beji, M. Reghima, M. Souli, N.K. Turki, Alloys and Compounds 675, 231 (2016); https://doi.org/10.1016/j.jallcom.2016.03.115
[24] S. Chatterjee, S.K. Saha, A.J. Pal, Solar Energy Materials and Solar 147, 17 (2016); https://doi.org/10.1016/j.solmat.2015.11.045
[25] F.J. Garcia-Garcia, P. Salazar, F. Yubero, A.R. González-Elipe, ElectrochimicaActa 201, 38 (2016); https://doi.org/10.1016/j.electacta.2016.03.193
[26] N. Ali, A. Hussain, R. Ahmed, M.K. Wang, C. Zhao, B. UlHaq, Y.Q. Fu, Renewable and Sustainable Energy Reviews 59, 726 (2016);https://doi.org/10.1016/j.rser.2015.12.268
[27] L. Dahbi, C. Zaouche, Y. Benkrima, A. Gahtar, Tobacco Regulatory Science 9(1), 2819(2023).
[28] S. Benramache, B. Benhaoua, Superlattices and Microstructures 52(16), 1062 (2012); https://doi.org/10.1016/j.spmi.2012.08.006
[29] O. Bayram, E. Sener, E. İgman. O. Simsek, Journal of Materials Science Materials in Electronics 30, 3452(2019); https://doi.org/10.1007/s10854-018-00620-2
[30] C. Zaouche, S. Benramache, International Journal of Advanced Multidisciplinary Research and Studies 3(5), 68(2023).
[31] A. Diha, S. Benramache, B.Benhaoua, Optik 172, 832(2018);https://doi.org/10.1016/j.ijleo.2018.07.062
[32] S. Benramache, Y. Aoun, S. Lakel, H. Mourghade, R. Gacem, B. Benhaoua, Journal of Nano- and Electronic Physics 10, 06032(2018);https://doi.org/10.21272/jnep.10(6).06032
[33] C. Zaouche, L. Dahbi, S. Benramache, A. Harouache, Y. Derouiche, M. Kharroubi, H. A. Haslouk, M. A. A. Banalhag, H. M. Alkhoja, Journal of Ovonic Research 19(2), 197(2023); https://doi.org/10.15251/JOR.2023.192.197
[34] W. Daranfed, M. S. Aida, A. Hafdallah, H. Lekiket, Thin Solid Films 518, 1082(2009);

https://doi.org/10.1016/j.tsf.2009.03.227
[35] A. Gahtar, S. Benramache, C. Zaouche, A. Boukacham, A. Sayah, Advances In Materials Science 20(3), 36(2020); https://doi.org/10.2478/adms-2020-0015
[36] S. Benramache, B. Benhaoua, F. Chabane, Journal of Semiconductors 33(9), 093001(2012); https://doi.org/10.1088/1674-4926/33/9/093001
[37] C. Zaouche, S. Benramache, A. Gahtar, Biomedical Journal of Scientific Technical Research 52(3), 43761(2023).
[38] C. Zaouche, A. Gahtar, S. Benramache, Y. Derouiche, M. Kharroubi, A. Belbel, C. Maghni, L. Dahbi, Digest Journal of Nanomaterials and Biostructures 17(4), 1453(2022); https://doi.org/10.15251/DJNB.2022.174.1453
[39] S. Benramache, Y. Aoun, A. Charef, B. Benhaoua, S. Lake, Inorganic and Nano-Metal Chemistry 49, 177(2019); https://doi.org/10.1080/24701556.2019.1624568
[40] M. Othmane, A. Attaf, H. Saidi, F. Bouaichi, N. Lehraki, M. Nouadji, M. Poulain, S. Benramache, International Journal of Nanoscience 15, 1650007(2015); https://doi.org/10.1142/S0219581X16500071
[41] A. Gahtar, A. Benali, S. Benramache, C. Zaouche, Chalcogenide Letters 19(2), 103(2022); https://doi.org/10.15251/CL.2022.192.103